Quercetin Alleviates Demyelination to Mitigate Neuropsychiatric Symptoms Through Promoting Microglia M2 Polarization in Mice with Vascular Dementia

Zihu Tan
Hubei Provincial Hospital of Traditional Chinese Medicine
Guang Yang
Hubei Provincial Hospital of Traditional Chinese Medicine
Jing Qiu
Hubei Provincial Hospital of Traditional Chinese Medicine
Wenjing Yan
Hubei University of Chinese Medicine
Yu Liu
Hubei Provincial Hospital of Traditional Chinese Medicine
Zhengling Ma
Hubei University of Chinese Medicine
Jia Li
Hubei University of Chinese Medicine
Jing Liu
Hubei University of Chinese Medicine
Nan Shan (shannan0116@163.com)
Hubei Provincial Hospital of Traditional Chinese Medicine https://orcid.org/0000-0003-4251-8847

Research Article

Keywords: vascular dementia, Quercetin, oligodendrocyte, microglia, neuropsychiatric symptoms

Posted Date: November 1st, 2021

DOI: https://doi.org/10.21203/rs.3.rs-1030799/v1

Abstract

Cerebral hypoperfusion plays a pivotal role in the ictus and development of vascular dementia (VaD) with neuropsychiatric symptoms. To date, few pharmacological interventions for neuropsychiatric symptoms are available in the VaD patients with neuropsychiatric impairments. Here, our results demonstrated that the extent of demyelination was dramatically deteriorated and the thickness of myelin sheath were evidently decreased in the presence of cerebral hypoperfusion, whereas Quercetin possessed the potential of abrogating these effects at least in part, then relieving anxiety and depression-like behavior when mice exposed to bilateral carotid artery stenosis (BCAS)/chronic restraint stress (CRS). The underlying mechanism was that Quercetin facilitated microglia transformation into M2 phenotype, which expedited secretion of anti-inflammatory cytokines (IL-4 and IL-10), and in turn decreased production of pro-inflammatory factors (TNF-α and IL-1β), thereafter enhancing the microglial engulfment ability of myelin fragments in vitro and in vivo. Collectively, the results demonstrated that that Quercetin facilitated microglia transition into M2 phenotype to reduce demyelination in ventral hippocampus (vHIP), thereafter mitigating neuropsychiatric deficits (including anxiety and depression). The present research broadens the therapeutic scope of Quercetin in central nervous system (CNS) disorders with presence of white matter damage and/or the insufficient activation of M2 microglia, particularly for vascular dementia with/without neuropsychiatric symptoms.

Introduction

Vascular dementia (VaD) is the second leading cause of dementia [1]. Cerebral hypoperfusion plays a pivotal role in the ictus and development of VaD. Our previous study has indicated that rats are susceptible to suffering from neuropsychiatric symptoms such as anxiety and depression when they are exposed to chronic restraint stress (CRS) in rats with bilateral common carotid arteries occlusion (BCCAO) introducing cerebral hypoperfusion [2]. Meanwhile, a positive loop exists between the severity of dementia and neuropsychiatric deficits, that is the severity of dementia aggravates as neuropsychiatric impairments progress, and vice versa [3]. However, few pharmacological interventions for neuropsychiatric symptoms are available in the treatment of VaD patients with neuropsychiatric impairments [4]. Recently, researches represent that cerebral hypoperfusion resulting from carotid artery stenosis contributes to neuropsychiatric insults in Alzheimer's disease (AD), aging, and vascular cognitive impairment (VCI) by causing damage to white matter bundles [5–7]. Additionally, studies have demonstrated that the severity of neuropsychiatric symptoms is positively correlated with the extent of demyelination in AD and multiple sclerosis (MS) [8, 9]. Hence, exploiting therapeutic strategies to alleviate demyelination or to preserve white matter integrity might be an applicable method to mitigate VaD-associated neuropsychiatric symptoms.

Quercetin is an important flavonoid component extracted from a wide range of traditional Chinese herbs [10], and exerts various pharmacological benefits, including anti-oxidant, anti-inflammatory, anti-viral and anti-tumor effects [10–14]. Currently, previous investigations have showed that Quercetin holds the potential of protecting neurons against ischemic insult [15], amyloid β-peptide (1-42)-induced cytotoxicity

[16, 17] and oxidative stress [18]. Meanwhile, researches reveal that quercetin inhibits depression-like behavior by suppressing astrocytes activation, proliferation and migration to reduce glial scar formation [19, 20]. Furthermore, cumulating evidence recapitulates that Quercetin promotes oligodendrocyte precursor cells (OPCs) expansion, and attenuating OPCs apoptosis in vitro under oxygen/glucose deprivation (OGD) condition [17, 21, 22]. Additionally, previous report illustrates that Quercetin application improves functional recovery through preventing demyelination, and boosting myelin repair after optic chiasm injury [23]. These investigations state a fact that Quercetin exerts multiple neuroprotective effects after central nervous system (CNS) injury. Most recently, research has demonstrated that Quercetin hinders necroptosis of oligodendrocytes through attenuating macrophages/microglia transition into M1 phenotype following spinal cord injury (SCI) in rats [10], implying that microglial shift resulting from Quercetin might be involved in mediating microglial transformation to diminish oligodendrocytes loss after CNS injury. However, whether quercetin holds the potential of mitigating neuropsychiatric symptoms induced by demyelination in the VaD patients through promoting microglial phenotype transition remains ambiguous.

With respect to that ventral hippocampus (vHIP), which is a key node in brain circuits modulating stress susceptibility through white matter fibers projections [24], usually suffers from demyelination when exposed to cerebral hypoperfusion as hippocampus is sensitive to ischemia [25]. Our previous study has illustrated that rats are susceptible to encountering neuropsychiatric symptoms including anxiety and depression by reducing dendritic spine density, length and branches in hippocampal cornu ammonis (CA1) and dentate gyrus (DG) of hippocampus when rats are exposed to cerebral hypoperfusion using a model of BCCAO [2]. In the present study, we speculated that Quercetin held the capacity of mitigating neuropsychiatric symptoms including anxiety and depression through alleviating demyelination in vHIP, and the underlying mechanism is that Quercetin boosts microglia polarization into M2 phenotype to potentiate phagocytosis in vHIP. Then, a model of bilateral carotid artery stenosis (BCAS) was established to introduce cerebral hypoperfusion in mice, and CRS was performed to induce neuropsychiatric impairments. Thereafter, Quercetin was administrated to investigate its effect on neuropsychiatric deficits using behavioral tests in BCAS/CRS mice. Subsequently, the role of Quercetin in alleviating demyelination via microglial conversion was determined by immunofluorescence, western blotting, and transmission electron microscopy (TEM) in vitro and in vivo. The aim of the present study is to widen the therapeutic scope of Quercetin in VaD, and to provide a feasible candidate for treating VaD-associated neuropsychiatric disorders.

Material And Methods

Animals

This work was approved by Ethics Committee of Hubei Provincial Hospital of Traditional Chinese Medicine (approval no. HBZY2020-C47-01) and all experimental procedures were performed according to the Chinese Animal Welfare Legislation for protection of animals used for scientific purposes. Every effort was made to reduce animal suffering and to minimize the number of animals used in the present work. A

total of 40 male adult C57BL/6 (6-week-old, 24-30 g) mice were purchased from Experimental Animal Research Center of Hubei Province. All mice were housed on a constant temperature (21 ± 3 ℃), moisture (60 ± 5%), and photoperiod (12-h light/dark cycle) condition. All mice were allowed to free access to food and water before and after surgery.

Bilateral Carotid Artery Stenosis (BCAS)

Bilateral carotid artery stenosis (BCAS) surgery was performed as previously described [7,26]. Mice were anesthetized using isoflurane/air mixture (2 l/min). All surgical procedures were conducted under aseptic condition and body temperature was maintained at 37 ± 0.3 °C using a feedback-controlled heating system (Zhongshi, inc., Beijing, China) during surgery. In brief, a small cervical midline incision was introduced, and the bilateral carotid arteries were exposed under a stereomicroscope (SZM45, Sunny, NingBo, China). A 2.5 mm-long microcoil (0.18-mm internal diameter, 0.08-mm diameter, 0.5 mm thread pitch) was placed around one-side carotid artery. Subsequently, the mouse was allowed to recover for 30 minutes. The second microcoil was placed around the other carotid artery using the same method. In groups of Sham and Quercetin (Que), surgery was carried out in the same approach except for the placement of microcoils around bilateral carotid arteiries in mice. After surgery, mice were randomly assigned into the following groups: Sham group (without BCAS/CRS, without Que administration), Que group (without BCAS/CRS, with Que administration), BCAS/CRS group (with BCAS/CRS, without Que administration), BCAS/CRS + Que group (with BCAS/CRS, with Que administration).

Chronic Restraint Stress (CRS)

Chronic restraint stress (CRS) is a common approach to introduce anxious and depressive symptoms in animal models with cerebral hypoperfusion, as previously described [2]. Hence, the CRS was imposed to mice after BCAS surgery, and the effect of treatment on neuropsychiatric symptoms was investigated. CRS was performed to introduce cerebral hypoperfusion as previously described [27]. A mouse restraint system was daily applied for CRS from 9:00 to 15:00 lasting for consecutive 14 days. Briefly, each mouse was put into a 50 mL plastic tube with some breathing holes, which was well ventilated. There is a hopper at the front of the tube, which allowed restrained mice free access to food and water. Restrained mice were horizontally maintained in cages during the restraint sessions. Mice in the groups of Sham and Quercetin were kept in the cages without stress.

Drug Administration

Quercetin (Que) was purchased from Sigma-Aldrich (cat. no. Q4951, St. Louis, MO, USA). It was firstly dissolved in DMSO, then diluted in 0.9% saline. Que was intraperitoneally injected at the dose of 60 mg/kg body weight. In the Que group, mice daily received Que for 14 days. In the BCAS/CRS + Que group, mice received Que from the first day of CRS 1 hour before restraint stress once a day for 14 days. Mice in groups of Sham and BCAS/CRS received the same volume of DMSO and 0.9% saline as Que-treated mice.

Behavioral Tests

For behavioral tests, all experiments and analyses were performed by an individual investigator blinded to every designed group, and detailed procedures were demonstrated as follows.

For Morris Water Maze (MWM) test, all procedures were performed 2 weeks after surgery, as described previously [28,29]. Mice were trained 5 times each day at a 20-minute interval for 5 days. In each test, mice were given 90 seconds to find the platform. Swimming was video-tracked, and the mean escape latency was recorded as a major outcome. If the latency was more than 90 seconds, mice were randomly divided into group BCAS/CRS or group BCAS/CRS + Quercetin.

For Elevated Plus Maze (EPM) test, the instrument and procedures were stated in our previous report [2]. In brief, mice were placed in the central platform facing the open arm. Then, mice moving trace was recorded by a camera (Zhongshi, inc., Beijing, China) and analyzed using an automatic animal behavior analysis software (Yihong Technology, Wuhan, China).

For Open Field Test (OFT), mice were placed into the corner of an open arena (100 × 100 × 40 cm), and allowed to freely explore for 5 minutes. The arena was divided into 16 (4 × 4) equal-size squares and the middle nine grids (2 × 2) were considered as the central zone. Moving distance, time spent, and grooming times in the center of the arena were recorded by a camera (Yihong Technology, Wuhan, China). Thereafter, the behavioral records were analyzed by an AVTAS version 4.0 system (Yihong Technology, Wuhan, China).

For Tail Suspension Test (TST), the tail of mouse was fixed on a metal wire hook which was about 1 meter away from the ground. The immobility time of each mouse was recorded within 5 min, including the period when the whole body was shaking, the limb and head were relatively motionless. Mice were not allowed to climb up their tails and fall off the end of their tails during suspension. The total amount of immobility time was measured for each mouse, and considered as an index of “depression-like” behavior.

For Forced Swim Test (FST), mice were placed in a large graduated cylinder filled halfway with water. Primarily, mice exhibited a period of vigorous activity when the mice tried to escape. Eventually, mice gave up vigorous activity and represented a typical immobility in which they only moved to maintain its head above water. This physical immobility was considered as an indicator of behavioral despair. Investigators measured the amount of time between when mice were placed in the cylinder and the onset of immobility. Mice with depression exhibited a decrease in the time spent trying to escape.

For Sucrose Preference Test (SPT), mice were placed in their home cage for 3 days with presence of two drinking bottles (one containing plain drinking water and the other one containing 2% sucrose). Next, mice were permitted to free access to either drinking the plain water or 2% sucrose solution for a period of 4 days. Water and sucrose solution consumption was measured daily, and the position of two bottles was changed daily to reduce any confound produced by a side bias. Sucrose preference was represented

as a percentage of the volume of sucrose intake over the total volume of fluid intake and averaged over the 4 days of testing.

Primary Microglia Culture

Primary microglia were harvested from postnatal day 0-2 C57BL/6 mice as previously described [30,31]. Briefly, after removal of the meninges and cortical tissues under a dissecting microscope, hippocampi were incubated in enzymatic solution (1.2 M glucose, 100 mM MgSO4, 0.25 M EGTA, 200 U or 0.47 mg/ml DNase I, 0.48 mM Papain) for digestion at 37 °C for 30minutes. Then, the samples were triturated using a fire-polished Pasteur pipette and passed through a 70-μm Nylon cell strainer (Nest, Wuxi, Jiangsu, China) after they were rinsed twice with Dulbecco's modified Eagle's medium/nutrient mixture F-12 (DMEM/F12; Gibco, Grand Island, NY, USA). Thereafter, the mixed cell suspension was seeded on a T75 cell culture flask precoated with poly-L-lysine (PLL, Sigma) in DMEM/F12 containing 10% FBS (Gibco, Grand Island, NY, USA) and 1% penicillin/streptomycin after being centrifuged at 1,500 rpm for 5 minutes. The cells were cultured in a constant-temperature incubator (Sanyo, Osaka, Japan) at 37 °C under 5% CO_2 humidified condition. Microglia were isolated from primary mixed glial cell cultures on day 8 by shaking the flasks 1 hour at 150 rpm on a rotary shaker at 37°C. Afterwards, the detached microglial cells were reseeded into cell culture plates at a density of 5×10^5 cells/ml in complete cell culture medium. The purity of the microglia was more than 90% that were confirmed by immunostaining with the microglial marker Iba1.

For microglia treatment, Que (cat. no. S2391, Selleck, Houston, TX, USA) was dissolved in DMSO and diluted to the working concentration with culture medium. The microglia were assigned into the following 6 groups: Control, Que 30 μM, Que 60 μM, OGD, OGD + Que 30 μM; (6) OGD + Que 60 μM. The same amount of DMSO was added in each group as the groups of Que 60 μM and OGD + Que 60 μM.

Oxygen-Glucose Deprivation and Reoxygenation (OGD/R)

A hypoxia chamber was performed according to the procedures of OGD as previously described [31,2]. Before the experiment, microglial cells were washed twice by PBS and immersed in serum-and glucose-free Dulbecco's modified Eagle's medium (DMEM; Gibco, Grand Island, NY, USA). Then, they were placed in the hypoxia chamber with a premixed gas (1% O2, 94% N2, 5% CO2) at 37°C. Two hours later, the OGD was terminated by bringing the plates back to a normoxic chamber after culture medium were exchanged to prewarmed DMEM/F12 supplemented with 10% FBS (Gibco, Grand Island, NY, USA). To determine the effect of Que on microglial cells, microglial were pretreated with 30 μM or 60 μM Que for 2h prior to OGD and presented during the whole experiment of OGD/R. Microglia in Control group were incubated under normal condition during the procedures without exposure to OGD.

Myelin Fragments Isolation

The myelin fragments were isolated as previously described [32]. In short, hippocampi were dissected from whole brains collected from five young adult C57BL/6 mice and myelin fragments was isolated

using a discontinuous sucrose gradient. Hippocampi were homogenized using 20 ml 0.32 M sucrose and 10 ml of lysis was layered between 18.5 ml 0.85 M sucrose and 8.5 ml 0.32 M sucrose. Thereafter, the suspension was ultracentrifuged at 75000 g for 20 minutes without brake. Subsequently, the interface was collected, homogenized in 35 ml distilled water, and ultracentrifuged at 75000 g for a further 15 minutes. The supernatant was aspirated and the pellet re-suspended in 35 ml distilled water. Afterwards, the suspension was ultracentrifuged at 12000 g for 10 minutes. The pellet was re-suspended in 10 ml 0.32 M sucrose, layered over 20 ml 0.85 M sucrose in a clean tube and then ultracentrifuged at 75000 g for 30 minutes. Finally, the interface was collected and centrifuged at 16000 g for 15 minutes to collect the myelin fragments that was stored at -80 °C for future experiments under sterile condition.

Transmission Electron Microscopy (TEM)

TEM was carried out as previously described [2]. The mouse ventral hippocampi (vHIP) tissues from each group were incubated in 2.5% glutaraldehyde for 4 hours at 4℃. Then, the samples were fixed in 1% citric acid for 2 hours at 20 °C. Afterwards, the specimens were dehydrated with gradient acetone after soaking in uranyl acetate. Thereafter, samples were embedded with epoxy resin and sliced into 70 nm, and counterstained with lead citrate after placing on the copper trough grid. Subsequently, the ultrastructure of axon caliber and myelinated axons was observed using a transmission electron microscope Tecnai G220 (FEI, Hillsboro, OR, USA). Myelinated axons were counted in all 5 images per vHIP, and the G-ratio and axon caliber of all myelinated axons perpendicular to the field of view were determined using ImageJ and the ImageJ distribution Fiji, as previously described [33]. All data were analyzed and counted by two investigators blind to sample information.

Klüver-Barrera Luxol Fast Blue (LFB) Staining

The frozen brain sections from each group were soaked in 0.1% Luxol Fast Blue (LFB) staining solution overnight at 28 °C. Then, the surplus dye solution was rinsed with 95% ethanol on the next day. Next, the samples were differentiated in 0.05% Lithium Carbonate Solution for 30 seconds after being washed with distilled water. Thereafter, the specimens were re-differentiated with 70% ethanol and transparented by xylene. Afterwards, the slides were observed using a light microscopy after being mounted with resinous medium. The spared myelin in white matter was examined using Image pro-plus (Media Cybernetics, Silver Spring, USA). The classification score according to the degree of myelin morphology damage was as follows: grade 0 (0 points), the myelin fibers were arranged in an orderly manner; grade 1 (1 point), the myelin fibers were arranged disorderly; grade 2 (2 points), vacuoles were formed in the myelin sheath; grade 3 (3 points): Myelin fibers disappeared.

Western Blotting

The whole lysate was extracted from microglia or hippocampi in different groups, and the concentration was determined by a BCA kit (Beyotime, Shanghai, China) according to the manufacturer's instruction. Then, samples were separated by electrophoresis using 8% or 10% SDS-PAGE, and transferred onto polyvinylidene difluoride (PVDF) membranes (Millipore, Burlington, MA). Subsequently, membranes

were incubated in primary antibodies at 4°C overnight after they were blocked with 5% skim milk or 5% BSA at room temperature for 2 hours. Thereafter, membranes were incubated in horseradish peroxidase (HRP)-conjugated secondary antibody at room temperature for 2 hours after rinsed twice with TBST. The signals for every band were detected using ECL luminous fluid (Beyotime, Shanghai, China) by a ChemiDoc™ XRS$^+$ imaging system (Bio-Rad, California, USA). Densitometric measurement of each membrane was performed using ImageJ. The primary antibodies used in the present study were as follows: MBP (1:1000, cat. no. 78896s, Cell Signaling Technology, Danvers, MA, USA), MAG (1:1000, cat. no. 114386-1-AP, Proteintech Group, Inc, Wuhan, China), MOG (1:1000, cat. no. 12690-1-AP, Proteintech Group, Inc, Wuhan, China), IL-4 (1:1000, cat. no. 66142-1-Ig, Proteintech Group, Inc, Wuhan, China), IL-10 (1:1000, cat. no. 60269-1-Ig, Proteintech Group, Inc, Wuhan, China), GAPDH (1:1000, cat. no. 60004-1-Ig, Proteintech Group, Inc, Wuhan, China), iNOS (1:1000, cat. no. 13120s, Cell Signaling Technology, Danvers, MA, USA), or Arg1 (1:1000, cat. no. 93668s, Cell Signaling Technology, Danvers, MA, USA), TNF-α (1:1000, cat. no. 11948, Cell Signaling Technology, Danvers, MA, USA), or IL-1β (1:1000, cat. no. 63124, Cell Signaling Technology, Danvers, MA, USA).

Immunofluorescence

For immunofluorescence, coverslips or frozen brain sections from each group were post-fixed using 4% paraformaldehyde (PFA) in 0.01 M phosphate buffer saline (PBS) for 30 minutes at room temperature after being twice washed with PBS. Then, the samples were incubated in 5% bovine serum album (BSA; Beyotime, Shanghai, China) solution supplemented with 0.3% Triton X-100 (Solarbio, Beijing, China) in PBS at room temperature for 2 hours. Thereafter, specimens were incubated in MBP (1:1000, cat. no. 78896s, Cell Signaling Technology, Danvers, MA, USA), iNOS (1:200, cat. no. 13120s, Cell Signaling Technology, Danvers, MA, USA), Iba1 (1:300, cat. no. 17198S, Cell Signaling Technology, Danvers, MA, USA), or Arg1 (1:200, cat. no. 93668s, Cell Signaling Technology, Danvers, MA, USA) overnight at 4˚C. On the next day, the specimens were incubated in Alexa Fluor® 555 or 488-conjugated secondary antibody (1:300; cat. nos. A0453 and A0423; Beyotime, Shanghai, China) at room temperature for 2 hours. Cell nuclei were counterstained with 4',6-diamidino-2-phenylindole (DAPI, Sigma-Aldrich, Munich, Germany) at room temperature for 10 minutes. Subsequently, sections were mounted onto slides and images were captured using a fluorescence microscopy (Zeiss, Göttingen, Germany). Meanwhile, blocking buffer without the primary antibodies was used as the negative control. Image-Pro Plus 6.0 software (Media Cybernetics, Inc., Rockville, MD, USA) was used for semi-quantitative analysis of immunostaining images. For each sample, at least twelve slices were analyzed, and the cross-sectional areas were calculated and reported as the average of four independent measurements. All measurements were performed by an individual investigator who was blinded to sample information.

Enzyme Linked Immunosorbent Assay (ELISA)

The secretion of cytokines of IL-1β, TNF-α, IL-10 and IL-4 was determined using ELISA. The same amount of 100 μl supernatant from each group were used to quantify the concentration of IL-1β (cat. no. DY401, R&D Systems, Minneapolis, MN, USA), IL-4 (cat. no. M4000B, R&D Systems, Minneapolis, MN, USA), TNF-

α (cat. no. DY410, R&D Systems, Minneapolis, MN, USA), and IL-10 (cat. no. M1000B, R&D Systems, Minneapolis, MN, USA) according to the manufacturer's instructions. Each experiment was repeated six times.

Statistical Analysis

Data were presented as mean ± SE, and analyzed using GraphPad Prism 6.0 software (GraphPad Software, Inc., San Diego, CA, USA) or SPSS 19.0 software (SPSS Inc., Chicago, IL, USA). The normal distribution of data was tested a using a Shapiro–Wilk normality test, and the significance of difference was determined by two-way analysis of variance (ANOVA) followed by Tukey's post hoc test. Statistical significance was represented as $p < 0.05$ ($^{*/\#}$), or $p < 0.01$ ($^{**/\#\#}$).

Results

Quercetin mitigated neuropsychiatric symptoms (including anxiety and depression) in BCAS/CRS mice.

The surgical strategy of bilateral carotid artery stenosis (BCAS) is a well-established method successfully introducing cerebral hypoperfusion [7]. Our previous study has illustrated that rats suffering from cerebral hypoperfusion are susceptible to encountering neuropsychiatric disorders including anxiety and depression when rats exposed to chronic restraint stress (CRS) for 14 days [2]. Herein, the model of BCAS supplemented with CRS for 14 days in mice was used to investigate the effect of Quercetin on neuropsychiatric symptoms including anxiety and depression in the present study. Considering that elevated plus maze (EPM) test is widely used for assessing anxious behavior in BCAS/CRS mice, we firstly performed EPM test in each group. Our results indicated that mice in group BCAS/CRS evidently decreased percentage of open arm time (Figure 1A, B), open arm entries (Figure 1A, C), and stretching number (Figure 1A, D), while 60 mg/kg Quercetin significantly abrogated these effects (Figure 1A-D). Then, the OPT was further performed to certify the effect of TMP on anxious behavior improvement. The results demonstrated that mice in group BCAS/CRS dramatically reduced the distance (Figure 1E, F) and duration (Figure 1E, G) in the center, and diminished the grooming times (Figure 1E, H), whilst 60 mg/kg Quercetin obviously abolished these effects (Figure 1E-H). Together, these results showed that 60 mg/kg Quercetin held the capacity of improving anxiety-like behavior in BCAS/CRS mice.

Furthermore, the effect of Quercetin on depression-like behavior in BCAS/CRS mice was investigated using tail suspension test (TST), forced swimming test (FST), and sucrose preference test (SPT). Initially, the results recapitulated that mice in group BCAS/CRS prominently increased the immobility time, and 60 mg/kg Quercetin profoundly reversed this situation (Figure 2A). Meanwhile, the FST was performed to certify the results obtained from TST. The results indicated that the immobile period in BCAS/CRS mice was markedly prolonged, while 60 mg/kg Quercetin obviously decreased the immobile duration (Figure 2B). Subsequently, SPT was carried out to evaluate the role of Quercetin in mediating depression-like behavior in BCAS/CRS mice. The results demonstrated that the percentage of sucrose preference was surely diminished in BCAS/CRS mice, whereas administration of 60 mg/kg Quercetin remarkably elevated

the percentage of sucrose consumption (Figure 2C). Collectively, these results demonstrated that 60 mg/kg Quercetin possessed the ability of ameliorating anxiety and depression-like behavior induced by BCAS combined with CRS in mice.

Quercetin alleviated ventral hippocampal demyelination in BCAS/CRS mice.

With respect to the ventral hippocampus (vHIP) is a key node in brain circuits modulating stress susceptibility through white matter fibers projections [24], and cerebral hypoperfusion always causes demyelination [34, 7], we posited that mice suffering from BCAS/CRS might exhibit demyelination in vHIP. Firstly, the expression of myelin-associated proteins (including MBP, MAG and MOG) was determined using western blotting assays. The bands illustrated that the expression of MBP, MAG and MOG was significantly decreased in vHIP after BCAS/CRS in mice, while 60 mg/kg Quercetin partially reversed this effect, that was 60 mg/kg Quercetin upregulated the myelin-associated protein expression (Figure 3A-D). Then, Klüver-Barrera Luxol fast blue (LFB) staining was performed to visualize the distribution of myelin sheath in vHIP. The images depicted that the damage score was obviously elevated in group BCAS/CRS than that in Sham and Que groups, whereas administration of 60 mg/kg Quercetin could reduce the damage score in vHIP (Figure 3E, F). Afterwards, the optical density of MBP in vHIP was assessed in each group using immunofluorescence. The immunostaining images showed that the optical density of MBP in vHIP was evidently reduced in group BCAS/CRS, nevertheless it was dramatically upregulated with administration of 60 mg/kg Quercetin (Figure 4A, B). Subsequently, the myelinated axons in vHIP were assessed using SEM. To optimize the measurement of myelin sheath thickness, we first plotted the efficiency index curves for axon caliber as previously described [35]. The results represented that the axon caliber in groups Sham and Que showed no statistical difference (Figure 4C, D), and no obvious significance in groups BCAS/CRS and BCAS/CRS + Que (Figure 4C, E). However, the G-ratio of myelin sheath was prominently increased in group BCAS/CRS, while it was dramatically reduced with the treatment of 60 mg/kg Quercetin (Figure 4C, F). Together, these results indicated that mice received BCAS/CRS could induce demyelination, whereas Quercetin partially restored myelination in vHIP.

Quercetin facilitated microglial shift from M1 to M2 phenotype in vHIP after mice suffering from BCAS/CRS.

Considering that Quercetin is an anti-inflammatory mediator after central nervous system (CNS) injury such as spinal cord injury (SCI) [10] and ischemic stroke [36], we hypothesized that Quercetin might involve in regulating neuroinflammation in mice suffering from BCAS/CRS. The western blotting assays were firstly performed to uncover the reason why Quercetin preserves myelination in vHIP. The bands exhibited that the expression of iNOS, one of M1 markers, was obviously increased after mice encountered BCAS/CRS (Figure 5A, B). However, the elevated expression of iNOS was reduced, and the expression of Arg-1, one of M2 markers, was significantly upregulated in vHIP after mice exposed to BCAS/CRS (Figure 5A, C). Thereafter, the immunostaining was carried out to verify the immunoblots results. The immunostaining images revealed that the percentage of $iNOS^{+}Iba1^{+}/Iba^{+}$ cells was substantially increased in vHIP after mice exposed to BCAS/CRS, and the percentage was reduced with

administration of 60 mg/kg Quercetin (Figure 5D, E). Meanwhile, the percentage of $Arg1^+Iba1^+/Iba^+$ cells was a bit higher in group BCAS/CRS, and the highest percentage was present in group BCAS/CRS + Que (Figure 5F, G). Mechanically, these results illustrated that Quercetin promoted microglial M2 polarization in vHIP with mice exposure to BCAS/CRS.

Quercetin inhibited pro-inflammatory factors secretion and facilitated anti-inflammatory factors secretion to potentiate phagocytosis induced by microglial M2 shift.

The aforementioned results attained that Quercetin held the ability of promoting microglial transformation from M1 to M2 in vHIP after BCAS/CRS. The secretion of pro-inflammatory factors (IL-1β and TNF-α) by M1 phenotype and anti-inflammatory factors (IL-10 and IL-4) produced in microglial M2 was assessed using western blotting. The bands depicted that the expression of IL-1β and TNF-α was significantly increased in vHIP after mice exposed to BCAS/CRS, while 60 mg/kg Quercetin reversed this phenomenon at a higher level, compared to groups Sham and Que (Figure 6A-C). Meanwhile, the results indicated that the expression of IL-10 and IL-4 was higher in group BCAS/CRS than that in groups Sham and Que (Figure 6A, D, E), and the highest expression level of IL-10 and IL-4 was observed in group BCAS/CRS + Que (Figure 6A, D, E). Subsequently, the immunostaining was conducted to examine the phagocytosis of microglia using double-immunostaining MBP and Iba1 in vHIP in each group. The images showed that the percentage of MBP^+Iba1^+/Iba^+ cells was a bit higher in group BCAS/CRS, and the highest percentage was observed in group BCAS/CRS + Que (Figure 6F, G), implying that Quercetin might strengthen microglial phagocytosis initiated by microglial M2 transformation.

To verify this hypothesis, primary microglia were cultured in vitro, and various concentration of Quercetin was used to evaluate the effect of Quercetin on microglial polarization under oxygen-glucose deprivation and reoxygenation (OGD/R) condition. Firstly, the bands recapitulated that the expression of iNOS was exclusively elevated under OGD, while 30 μM and 60 μM Quercetin could downregulate the expression of iNOS (Figure 7A, B). Meanwhile, the expression of Arg1 was a bit higher under OGD, but no statistical difference was observed among groups of Control, 30 μM and 60 μM Quercetin without OGD (Figure 7A, C). However, the expression of Arg1 was remarkably elevated with administration of 30 μM and 60 μM Quercetin, and 60 μM Quercetin exhibited a better effect compared with 30 μM Quercetin (Figure 7A, C). Subsequently, the double-labelled of iNOS and Iba1 in primary microglia was carried out. The immunostaining images showed that the percentage of $iNOS^+/Iba1^+$ cells was diminished with treatment of 30 μM and 60 μM Quercetin without OGD (Figure 7D, E), while the ratio was substantially increased under OGD (Figure 7D, E), suggesting that OGD potentiated microglia conversion into M1 phenotype. The condition was overturned with addition of 30 μM and 60 μM Quercetin, and 60 μM Quercetin reported better efficacy (Figure 7D, E). Meantime, the proportion of $Arg1^+/Iba1^+$ cells was surely increased with administration of 30 μM and 60 μM Quercetin without OGD (Figure 7F, G). Under OGD condition, the portion was a bit higher than Control (Figure 7F, G), whereas the percentage of $Arg1^+/Iba1^+$ cells was profoundly increased with treatment of 30 μM and 60 μM Quercetin, and 60 μM Quercetin delineated

better effect (Figure 7F, G). Collectively, these results demonstrated that Quercetin facilitated M1-to-M2 transition with/without OGD in vitro.

In addition, the concentration of pro-inflammatory and anti-inflammatory cytokines secreted by microglia in supernatant was evaluated using ELISA assays. The results demonstrated that the content of IL-1β and TNF-α was dramatically increased under OGD, while this effect was declined with addition of 30 μM and 60 μM Quercetin, and 60 μM Quercetin displayed lower concentration (Figure 8A, B). Meanwhile, the concentration of IL-10 and IL-4 was the highest when microglia were treated with 60 μM Quercetin among all groups, and higher when microglia exposed to 30 μM Quercetin under OGD (Figure 8C, D). The concentration of IL-10 and IL-4 was slightly increased as microglia were exposed to OGD, but no significant difference was observed among groups without OGD, even with addition of 30 μM and 60 μM Quercetin (Figure 8C, D). Thereafter, the myelin fragments were isolated and the phagocytosis of microglia was investigated. The immunostaining images revealed that the percentage of MBP^+Iba1^+/Iba^+ cells was predominantly increased with administration of 30 μM and 60 μM Quercetin without OGD, and 60 μM Quercetin exhibited the most percentage of MBP^+Iba1^+/Iba^+ cells (Figure 8E, F), indicating that Quercetin held the capability of enhancing phagocytosis induced by microglial M2 transition without OGD. Subsequently, the proportion of MBP^+Iba1^+/Iba^+ cells was determined using immunostaining under OGD condition with presence of Quercetin. The results substantiated that the percentage of MBP^+Iba1^+/Iba^+ cells was significantly increased either with treatment of 30 μM Quercetin or 60 μM Quercetin (Figure G, H), and with no difference between these two treatments (Figure G, H). Mechanically, these results illustrated that Quercetin bore the potential of promoting phagocytosis through microglial M2 polarization with/without OGD.

Discussion

In the present research, our results demonstrated that the severity of demyelination was dramatically deteriorated and the thickness of myelin sheath were evidently decreased, whereas Quercetin possessed the potential of abrogating these effects at least in part, then relieving anxiety and depression-like behavior when mice exposed to BCAS/CRS. The underlying mechanism was that Quercetin facilitated microglia transformation into M2 phenotype, which assisted secretion of anti-inflammatory cytokines (IL-4 and IL-10) and in turn decreased production of pro-inflammatory factors (TNF-α and IL-1β), thereafter enhancing the microglial engulfment ability of myelin fragments in vitro and in vivo. Collectively, these results testified the hypothesis that Quercetin facilitated microglia transition to M2 phenotype to reduce demyelination in vHIP.

Microglia are resident macrophages in the CNS and act as the first-line guardian for the immune system within the brain parenchyma in physiological situation. Under pathological scenario, “classically activated” M1 microglia release pro-inflammatory cytokines (IL-1α, IL-1β, IL-6, IL-12, IL-23, TNF-α, iNOS) to initiate destructive effects, while “alternatively activated” M2 microglia produce a series of neuroprotective/neurotrophic factors, such as arginase-1 (Arg1), CD206, IL-4, IL-10, to facilitate phagocytosis of debris originated from injured and dead neural cells [37–39]. Previous investigation has

represented that Quercetin reduces the production of pro-inflammatory factors [17] ascribing to inhibiting microglia shift to M1 phenotype [10]. Here, our results present a proof that Quercetin bears the capacity of facilitating microglial M2 conversion, which enlarges the fundamental knowledge of Quercetin in mediating microglia activation. The M2 microglia subsequently increases the production of IL-4, one of the anti-inflammatory cytokines, suppressing local inflammation to diminish loss of local neural cells [39]. Furthermore, the elevated expression of IL-10 secreted by M2 microglia assists to decrease demyelination in mice with BCAS/CRS as previous study has delineated that IL-10 contributes to promoting oligodendrocytes myelination and functional recovery after SCI in mice [40].

Oligodendrocytes are the main subtype of neural cells responsible for myelination after CNS injury [41], and they are highly sensitive to hypoxic damage [42]. Here, the model of BCAS in mice was performed to introduce hypoxic injury, and CRS was imposed to initiate stress, which is an effective strategy to induce neuropsychiatric deficits following cerebral hypoperfusion [2]. The results substantiated that mice exposed to BCAS plus CRS exhibited severe anxiety and depression-like behavior due to myelin loss in vHIP, that could be partially mitigated with application of Quercetin, indicating that Quercetin turnovers the loss of mature oligodendrocytes and might potentiate the regenerative ability of OPCs, in a degree. Previous studies have demonstrated that cerebral hypoperfusion is one of the most common pathophysiological mechanism, which is a main cause to cognitive decline and neuropsychiatric symptoms progression in AD and VaD [43–45, 42]. However, unlike AD, there are no pharmacological treatments for VaD-associated neuropsychiatric symptoms. Our results provide evidence that ceasing the damage to white matter is a suitable therapeutic strategy for the treatment of VaD-associated neuropsychiatric impairments using Quercetin. Intriguingly, the results presented that Quercetin application under normal condition in mice, there was no obvious difference in white matter integrity and the engulfment capacity of M2 microglia, implying that Quercetin only exerts the microglial M2 polarization under pathological situation. Correspondingly, the present work provides an appropriate candidate for the treatment of neurodegenerative diseases existing demyelination and/or the insufficient activation of M2 microglia, even in other CNS diseases.

In sum, the present research substantiates a fact that Quercetin profoundly mitigates demyelination to lighten anxiety and depression-like behavior in mice suffering from BCAS plus CRS, and the underlying mechanism is potentiating microglial switch from M1 to M2 phenotype, which broadens the therapeutic scope of Quercetin in CNS disorders with presence of white matter damage and/or the insufficient activation of M2 microglia, particularly for vascular dementia with/without neuropsychiatric symptoms.

Abbreviations

VaD: vascular dementia

BCAS: bilateral carotid artery stenosis

CRS: chronic restraint stress

vHIP: ventral hippocampus

CNS: central nervous system

BCCAO: bilateral common carotid arteries occlusion

VCI: vascular cognitive impairment

MS: multiple sclerosis

AD: Alzheimer’s disease

OPCs: oligodendrocyte precursor cells

OGD: oxygen/glucose deprivation

SCI: spinal cord injury

CA1: hippocampal cornu ammonis

DG: dentate gyrus

TEM: transmission electron microscopy

LFB: Klüver-Barrera Luxol Fast Blue

PFA: paraformaldehyde

BSA: bovine serum album

DAPI: 4',6-diamidino-2-phenylindole

ELISA: enzyme linked immunosorbent assay

TST: tail suspension test

FST: forced swimming test

SPT: sucrose preference test

EPM: elevated plus maze

OFT: open field test

Declarations

Funding

This work was supported by grants from Wuhan Science and Technology Plan Application Foundation Frontier Project (2020020601012244).

Compliance with Ethical Standards

Disclosure of potential conflicts of interest

The authors have no relevant financial or non-financial interests to disclose.

Research involving Animals

This work was approved by Ethics Committee of Hubei Provincial Hospital of Traditional Chinese Medicine (approval no. HBZY2020-C47-01) and all experimental procedures were performed according to the Chinese Animal Welfare Legislation for protection of animals used for scientific purposes.

Informed consent

Not applicable.

Consent to participate

Not applicable.

Consent for Publication

Not applicable.

Author contributions

Z.H.T. performed most of the experiments. G.Y. and J.Q. analyzed the results. J.Q. and W.J.Y. edited figures. J.Q. and Y.L. performed mice BCAS model and statistical analysis. G.Y. and Z.L.M. performed cell culture and treatments. G.Y. and J.L. performed immunoblotting and immunostaining. Z.H.T. wrote preliminary draft of the manuscript. N.S. edited the manuscript. N.S. and Z.H.T. designed experiments and revised the manuscript. All authors approved final version of the manuscript.

Conflict of interest

The authors declare they have no conflict of interest.

Acknowledge

Not applicable.

Data Availability of data and materials

The data that support the findings of this study are available from the corresponding author upon reasonable request.

References

1. O'Brien JT, Thomas A (2015) Vascular dementia. Lancet 386 (10004):1698-1706. doi:10.1016/s0140-6736(15)00463-8
2. Tan Z, Qiu J, Zhang Y, Yang Q, Yin X, Li J, Liu G, Li H, Yang G (2021) Tetramethylpyrazine Alleviates Behavioral and Psychological Symptoms of Dementia Through Facilitating Hippocampal Synaptic Plasticity in Rats With Chronic Cerebral Hypoperfusion. Front Neurosci 15:646537. doi:10.3389/fnins.2021.646537
3. Savulich G, O'Brien JT, Sahakian BJ (2020) Are neuropsychiatric symptoms modifiable risk factors for cognitive decline in Alzheimer's disease and vascular dementia? Br J Psychiatry 216 (1):1-3. doi:10.1192/bjp.2019.98
4. Brodaty H, Arasaratnam C (2012) Meta-analysis of nonpharmacological interventions for neuropsychiatric symptoms of dementia. Am J Psychiatry 169 (9):946-953. doi:10.1176/appi.ajp.2012.11101529
5. Park JM, Kim YJ (2019) [Effect of Ghrelin on Memory Impairment in a Rat Model of Vascular Dementia]. J Korean Acad Nurs 49 (3):317-328. doi:10.4040/jkan.2019.49.3.317
6. Liu Q, Bhuiyan MIH, Liu R, Song S, Begum G, Young CB, Foley LM, Chen F, Hitchens TK, Cao G, Chattopadhyay A, He L, Sun D (2021) Attenuating vascular stenosis-induced astrogliosis preserves white matter integrity and cognitive function. J Neuroinflammation 18 (1):187. doi:10.1186/s12974-021-02234-8
7. Sigfridsson E, Marangoni M, Hardingham GE, Horsburgh K, Fowler JH (2020) Deficiency of Nrf2 exacerbates white matter damage and microglia/macrophage levels in a mouse model of vascular cognitive impairment. J Neuroinflammation 17 (1):367. doi:10.1186/s12974-020-02038-2
8. Kavroulakis E, Simos PG, Kalaitzakis G, Maris TG, Karageorgou D, Zaganas I, Panagiotakis S, Basta M, Vgontzas A, Papadaki E (2018) Myelin content changes in probable Alzheimer's disease and mild cognitive impairment: Associations with age and severity of neuropsychiatric impairment. J Magn Reson Imaging 47 (5):1359-1372. doi:10.1002/jmri.25849
9. Benedict RH, Bobholz JH (2007) Multiple sclerosis. Semin Neurol 27 (1):78-85. doi:10.1055/s-2006-956758
10. Fan H, Tang HB, Shan LQ, Liu SC, Huang DG, Chen X, Chen Z, Yang M, Yin XH, Yang H, Hao DJ (2019) Quercetin prevents necroptosis of oligodendrocytes by inhibiting macrophages/microglia polarization to M1 phenotype after spinal cord injury in rats. J Neuroinflammation 16 (1):206. doi:10.1186/s12974-019-1613-2
11. Xu D, Hu MJ, Wang YQ, Cui YL (2019) Antioxidant Activities of Quercetin and Its Complexes for Medicinal Application. Molecules 24 (6). doi:10.3390/molecules24061123

12. Tang SM, Deng XT, Zhou J, Li QP, Ge XX, Miao L (2020) Pharmacological basis and new insights of quercetin action in respect to its anti-cancer effects. Biomed Pharmacother 121:109604. doi:10.1016/j.biopha.2019.109604
13. Spagnuolo C, Moccia S, Russo GL (2018) Anti-inflammatory effects of flavonoids in neurodegenerative disorders. Eur J Med Chem 153:105-115. doi:10.1016/j.ejmech.2017.09.001
14. Sun Y, Li C, Li Z, Shangguan A, Jiang J, Zeng W, Zhang S, He Q (2021) Quercetin as an antiviral agent inhibits the Pseudorabies virus in vitro and in vivo. Virus Res 305:198556. doi:10.1016/j.virusres.2021.198556
15. Ghosh A, Sarkar S, Mandal AK, Das N (2013) Neuroprotective role of nanoencapsulated quercetin in combating ischemia-reperfusion induced neuronal damage in young and aged rats. PLoS One 8 (4):e57735. doi:10.1371/journal.pone.0057735
16. Ansari MA, Abdul HM, Joshi G, Opii WO, Butterfield DA (2009) Protective effect of quercetin in primary neurons against Abeta(1-42): relevance to Alzheimer's disease. J Nutr Biochem 20 (4):269-275. doi:10.1016/j.jnutbio.2008.03.002
17. Naeimi R, Baradaran S, Ashrafpour M, Moghadamnia AA, Ghasemi-Kasman M (2018) Querectin improves myelin repair of optic chiasm in lyolecithin-induced focal demyelination model. Biomed Pharmacother 101:485-493. doi:10.1016/j.biopha.2018.02.125
18. Ahmad A, Khan MM, Hoda MN, Raza SS, Khan MB, Javed H, Ishrat T, Ashafaq M, Ahmad ME, Safhi MM, Islam F (2011) Quercetin protects against oxidative stress associated damages in a rat model of transient focal cerebral ischemia and reperfusion. Neurochem Res 36 (8):1360-1371. doi:10.1007/s11064-011-0458-6
19. Zhang J, Ning L, Wang J (2020) Dietary quercetin attenuates depressive-like behaviors by inhibiting astrocyte reactivation in response to stress. Biochem Biophys Res Commun 533 (4):1338-1346. doi:10.1016/j.bbrc.2020.10.016
20. Yuan Z, Yao F, Hu Z, Sun S, Wu B (2015) Quercetin inhibits the migration and proliferation of astrocytes in wound healing. Neuroreport 26 (7):387-393. doi:10.1097/wnr.0000000000000352
21. Wang XQ, Yao RQ, Liu X, Huang JJ, Qi DS, Yang LH (2011) Quercetin protects oligodendrocyte precursor cells from oxygen/glucose deprivation injury in vitro via the activation of the PI3K/Akt signaling pathway. Brain Res Bull 86 (3-4):277-284. doi:10.1016/j.brainresbull.2011.07.014
22. Wu X, Qu X, Zhang Q, Dong F, Yu H, Yan C, Qi D, Wang M, Liu X, Yao R (2014) Quercetin promotes proliferation and differentiation of oligodendrocyte precursor cells after oxygen/glucose deprivation-induced injury. Cell Mol Neurobiol 34 (3):463-471. doi:10.1007/s10571-014-0030-4
23. Beckmann DV, Carvalho FB, Mazzanti CM, Dos Santos RP, Andrades AO, Aiello G, Rippilinger A, Graça DL, Abdalla FH, Oliveira LS, Gutierres JM, Schetinger MR, Mazzanti A (2014) Neuroprotective role of quercetin in locomotor activities and cholinergic neurotransmission in rats experimentally demyelinated with ethidium bromide. Life Sci 103 (2):79-87. doi:10.1016/j.lfs.2014.03.033
24. Muir J, Lopez J, Bagot RC (2019) Wiring the depressed brain: optogenetic and chemogenetic circuit interrogation in animal models of depression. Neuropsychopharmacology 44 (6):1013-1026.

doi:10.1038/s41386-018-0291-6

25. Haukvik UK, Tamnes CK, Söderman E, Agartz I (2018) Neuroimaging hippocampal subfields in schizophrenia and bipolar disorder: A systematic review and meta-analysis. J Psychiatr Res 104:217-226. doi:10.1016/j.jpsychires.2018.08.012
26. Wang M, Qin C, Luo X, Wang J, Wang X, Xie M, Hu J, Cao J, Hu T, Goldman SA, Nedergaard M, Wang W (2019) Astrocytic connexin 43 potentiates myelin injury in ischemic white matter disease. Theranostics 9 (15):4474-4493. doi:10.7150/thno.31942
27. Tian P, Zhu H, Qian X, Chen Y, Wang Z, Zhao J, Zhang H, Wang G, Chen W (2021) Consumption of Butylated Starch Alleviates the Chronic Restraint Stress-Induced Neurobehavioral and Gut Barrier Deficits Through Reshaping the Gut Microbiota. Front Immunol 12:755481. doi:10.3389/fimmu.2021.755481
28. Liu B, Kou J, Li F, Huo D, Xu J, Zhou X, Meng D, Ghulam M, Artyom B, Gao X, Ma N, Han D (2020) Lemon essential oil ameliorates age-associated cognitive dysfunction via modulating hippocampal synaptic density and inhibiting acetylcholinesterase. Aging (Albany NY) 12 (9):8622-8639. doi:10.18632/aging.103179
29. Higaki A, Mogi M, Iwanami J, Min LJ, Bai HY, Shan BS, Kukida M, Kan-No H, Ikeda S, Higaki J, Horiuchi M (2018) Predicting outcome of Morris water maze test in vascular dementia mouse model with deep learning. PLoS One 13 (2):e0191708. doi:10.1371/journal.pone.0191708
30. Zhang Z, Qin P, Deng Y, Ma Z, Guo H, Guo H, Hou Y, Wang S, Zou W, Sun Y, Ma Y, Hou W (2018) The novel estrogenic receptor GPR30 alleviates ischemic injury by inhibiting TLR4-mediated microglial inflammation. J Neuroinflammation 15 (1):206. doi:10.1186/s12974-018-1246-x
31. Ji J, Wang J, Yang J, Wang XP, Huang JJ, Xue TF, Sun XL (2019) The Intra-nuclear SphK2-S1P Axis Facilitates M1-to-M2 Shift of Microglia via Suppressing HDAC1-Mediated KLF4 Deacetylation. Front Immunol 10:1241. doi:10.3389/fimmu.2019.01241
32. Rawji KS, Young AMH, Ghosh T, Michaels NJ, Mirzaei R, Kappen J, Kolehmainen KL, Alaeiilkhchi N, Lozinski B, Mishra MK, Pu A, Tang W, Zein S, Kaushik DK, Keough MB, Plemel JR, Calvert F, Knights AJ, Gaffney DJ, Tetzlaff W, Franklin RJM, Yong VW (2020) Niacin-mediated rejuvenation of macrophage/microglia enhances remyelination of the aging central nervous system. Acta Neuropathol 139 (5):893-909. doi:10.1007/s00401-020-02129-7
33. Maas DA, Eijsink VD, Spoelder M, van Hulten JA, De Weerd P, Homberg JR, Vallès A, Nait-Oumesmar B, Martens GJM (2020) Interneuron hypomyelination is associated with cognitive inflexibility in a rat model of schizophrenia. Nat Commun 11 (1):2329. doi:10.1038/s41467-020-16218-4
34. Holland PR, Bastin ME, Jansen MA, Merrifield GD, Coltman RB, Scott F, Nowers H, Khallout K, Marshall I, Wardlaw JM, Deary IJ, McCulloch J, Horsburgh K (2011) MRI is a sensitive marker of subtle white matter pathology in hypoperfused mice. Neurobiol Aging 32 (12):2325.e2321-2326. doi:10.1016/j.neurobiolaging.2010.11.009
35. Chomiak T, Hu B (2009) What is the optimal value of the g-ratio for myelinated fibers in the rat CNS? A theoretical approach. PLoS One 4 (11):e7754. doi:10.1371/journal.pone.0007754

36. Le K, Song Z, Deng J, Peng X, Zhang J, Wang L, Zhou L, Bi H, Liao Z, Feng Z (2020) Quercetin alleviates neonatal hypoxic-ischemic brain injury by inhibiting microglia-derived oxidative stress and TLR4-mediated inflammation. Inflamm Res 69 (12):1201-1213. doi:10.1007/s00011-020-01402-5
37. Colonna M, Butovsky O (2017) Microglia Function in the Central Nervous System During Health and Neurodegeneration. Annu Rev Immunol 35:441-468. doi:10.1146/annurev-immunol-051116-052358
38. Voet S, Prinz M, van Loo G (2019) Microglia in Central Nervous System Inflammation and Multiple Sclerosis Pathology. Trends Mol Med 25 (2):112-123. doi:10.1016/j.molmed.2018.11.005
39. Hu X, Leak RK, Shi Y, Suenaga J, Gao Y, Zheng P, Chen J (2015) Microglial and macrophage polarization—new prospects for brain repair. Nat Rev Neurol 11 (1):56-64. doi:10.1038/nrneurol.2014.207
40. Smith DR, Dumont CM, Park J, Ciciriello AJ, Guo A, Tatineni R, Cummings BJ, Anderson AJ, Shea LD (2020) Polycistronic Delivery of IL-10 and NT-3 Promotes Oligodendrocyte Myelination and Functional Recovery in a Mouse Spinal Cord Injury Model. Tissue Eng Part A 26 (11-12):672-682. doi:10.1089/ten.TEA.2019.0321
41. Domingues HS, Cruz A, Chan JR, Relvas JB, Rubinstein B, Pinto IM (2018) Mechanical plasticity during oligodendrocyte differentiation and myelination. Glia 66 (1):5-14. doi:10.1002/glia.23206
42. Duncombe J, Kitamura A, Hase Y, Ihara M, Kalaria RN, Horsburgh K (2017) Chronic cerebral hypoperfusion: a key mechanism leading to vascular cognitive impairment and dementia. Closing the translational gap between rodent models and human vascular cognitive impairment and dementia. Clin Sci (Lond) 131 (19):2451-2468. doi:10.1042/cs20160727
43. Qin C, Fan WH, Liu Q, Shang K, Murugan M, Wu LJ, Wang W, Tian DS (2017) Fingolimod Protects Against Ischemic White Matter Damage by Modulating Microglia Toward M2 Polarization via STAT3 Pathway. Stroke 48 (12):3336-3346. doi:10.1161/strokeaha.117.018505
44. Fadda G, Armangue T, Hacohen Y, Chitnis T, Banwell B (2021) Paediatric multiple sclerosis and antibody-associated demyelination: clinical, imaging, and biological considerations for diagnosis and care. Lancet Neurol 20 (2):136-149. doi:10.1016/s1474-4422(20)30432-4
45. Uemura MT, Maki T, Ihara M, Lee VMY, Trojanowski JQ (2020) Brain Microvascular Pericytes in Vascular Cognitive Impairment and Dementia. Front Aging Neurosci 12:80. doi:10.3389/fnagi.2020.00080

Figures

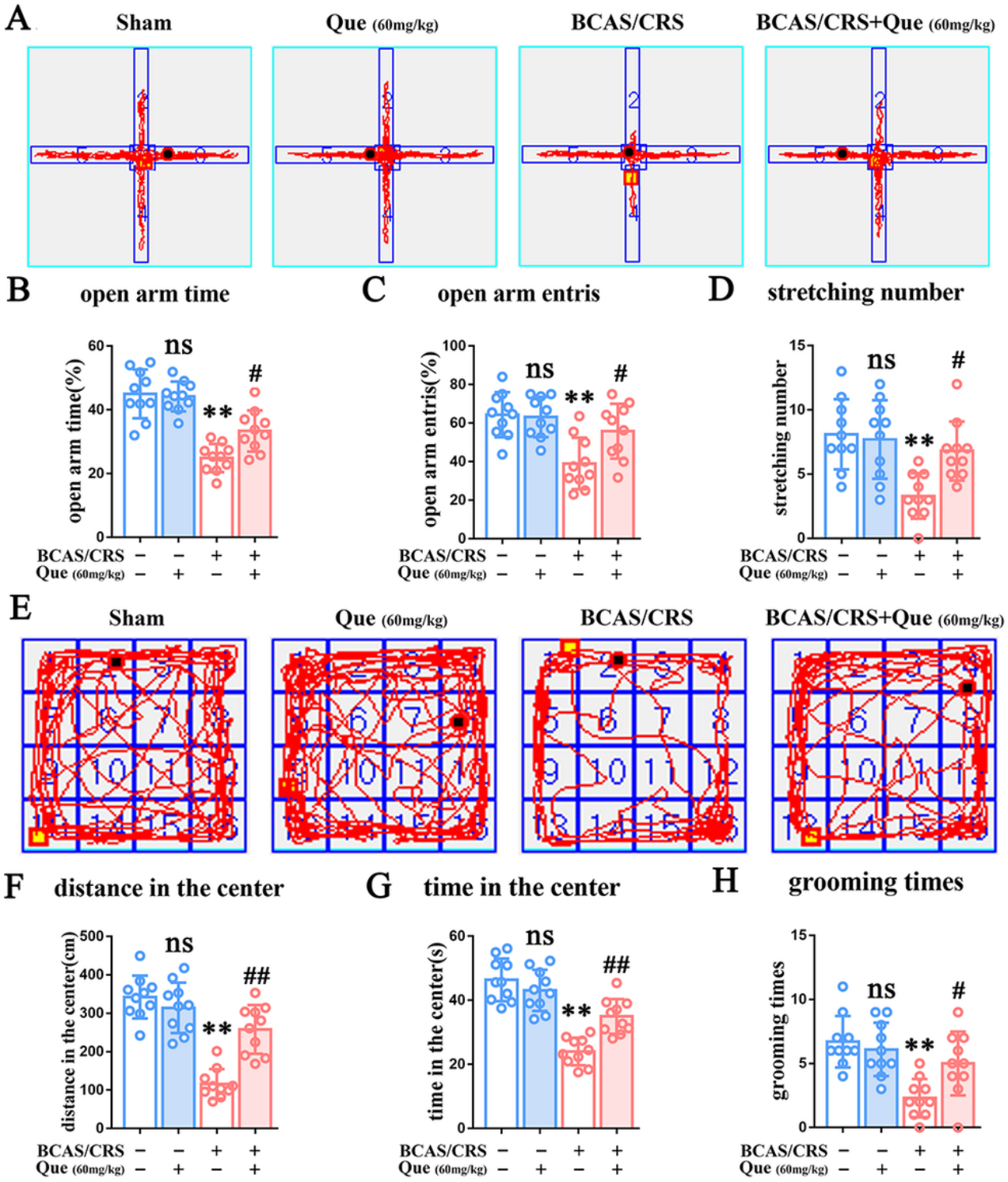

Figure 1

Quercetin alleviates anxiety-like behavior in BCAS/CRS mice. (A) Representational traces showing mice moving in the elevated plus maze (EPM) test. (B) Quantitative analysis of the percentage of time that mice were moving/staying in the open arms. (C) Quantitative analysis of the percentage of times that mice entered the open arms during EPM test. (D) Quantitation of the stretching number during EPM test. (E) Representational traces showing mice moving in the open filed test (OFT). (F) Quantitative analysis of

mice moving distance during the OFT. (G) Quantitative analysis of the duration that mice were moving/staying in the open filed. (H) Quantitation of the grooming number during OFT. N=10 in each group, *p<0.05, **p<0.01 versus sham; #p<0.05, ##p<0.01 versus BCAS/CRS; ns, no significant difference.

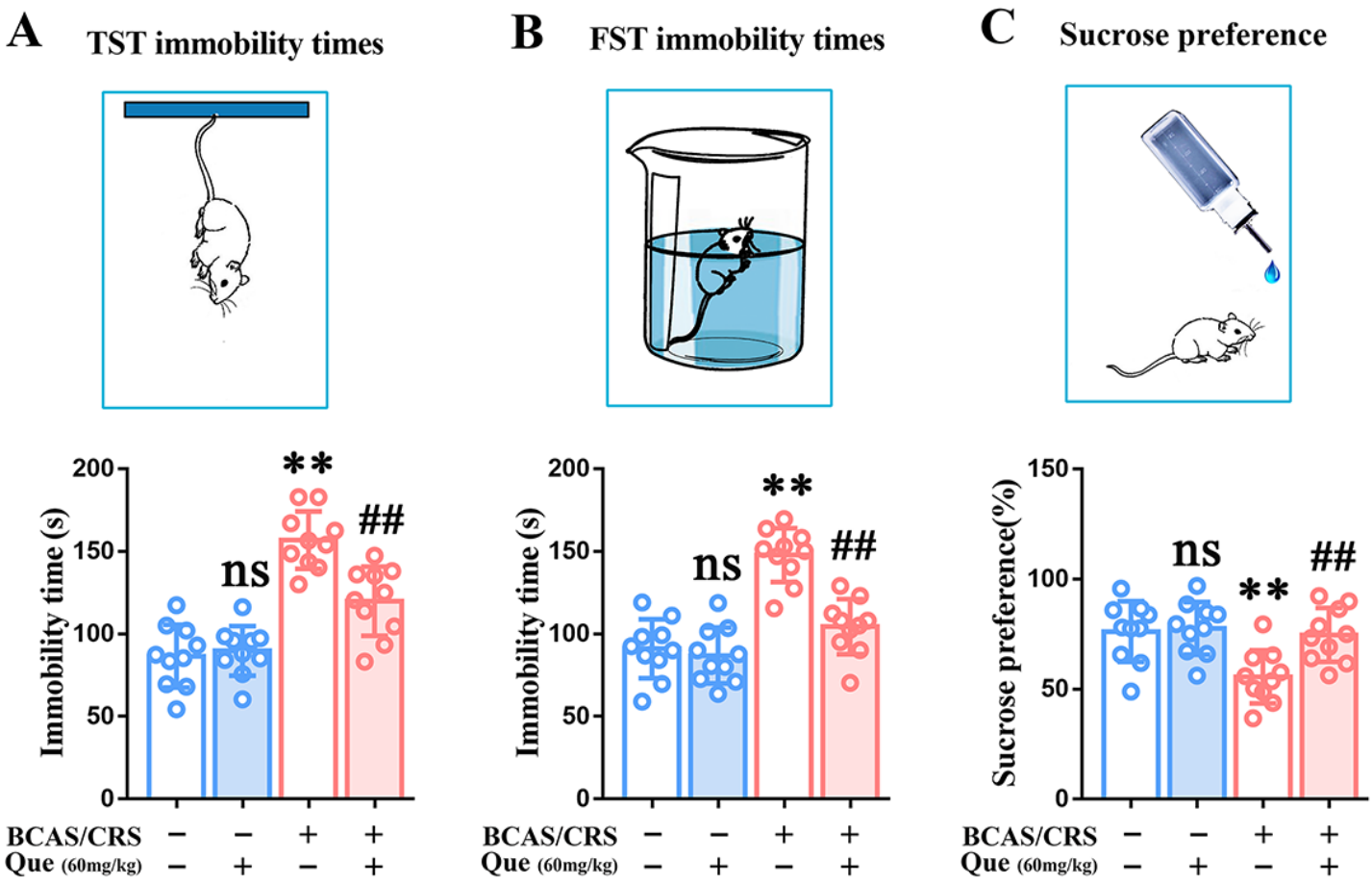

Figure 2

Quercetin relieves depression-like behavior in BCAS/CRS mice. (A) Schematic diagram of tail suspension test (TST) and statistical analysis summarizing the immobility time of mice in the TST. (B) Illustration of forced swimming test (FST) and histogram showing immobility time of mice in the FST. (C) Sketch of sucrose preference test (SPT) and bargraph representing the percentage of sucrose preference of mice in the FST. N=10 in each group, *p<0.05, **p<0.01 versus sham; #p<0.05, ##p<0.01 versus BCAS/CRS; ns, no significant difference.

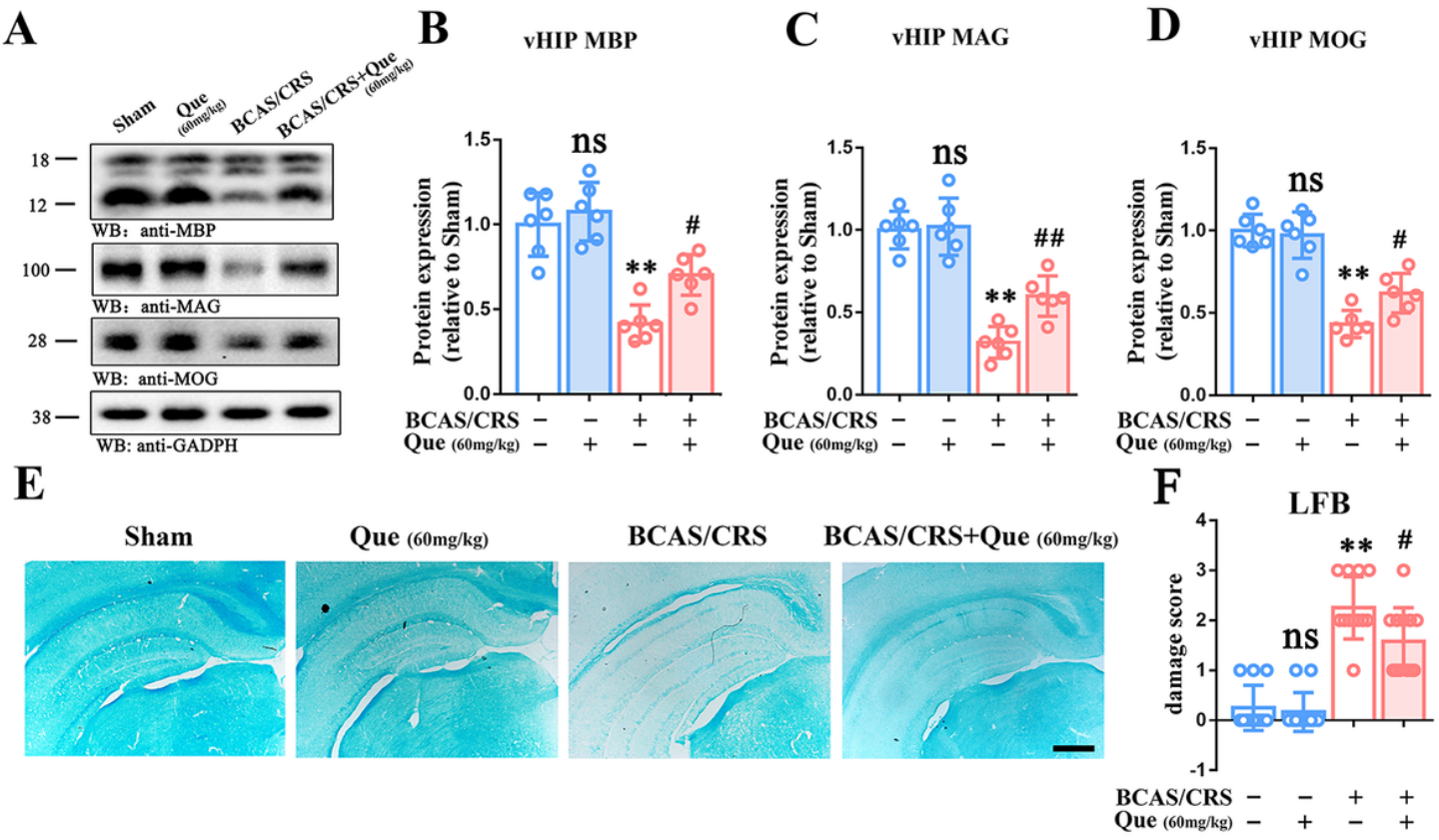

Figure 3

Quercetin mitigates ventral hippocampal demyelination in BCAS/CRS mice. (A) Representative immunoblots representing the expression of MBP, MAG and MOG in ventral hippocampus (vHIP). (B-D) Semi-quantitative analysis of myelin associated proteins including MBP (B), MAG (C), and MOG (D). N=6 in each group, *p<0.05, **p<0.01 versus sham; #p<0.05, ##p<0.01 versus BCAS/CRS; ns, no significant difference. (E) Myelin sheath was detected by Klüver-Barrera Luxol fast blue staining (LFB) in each group. Scale bar, 100 μm. (F) Semiquantitative scoring of demyelination (loss of LFB staining) in various groups. N=4 in each group, three brain slices per each sample were chosen for analysis. **p<0.01 versus sham; #p<0.05 versus BCAS/CRS; ns, no significant difference.

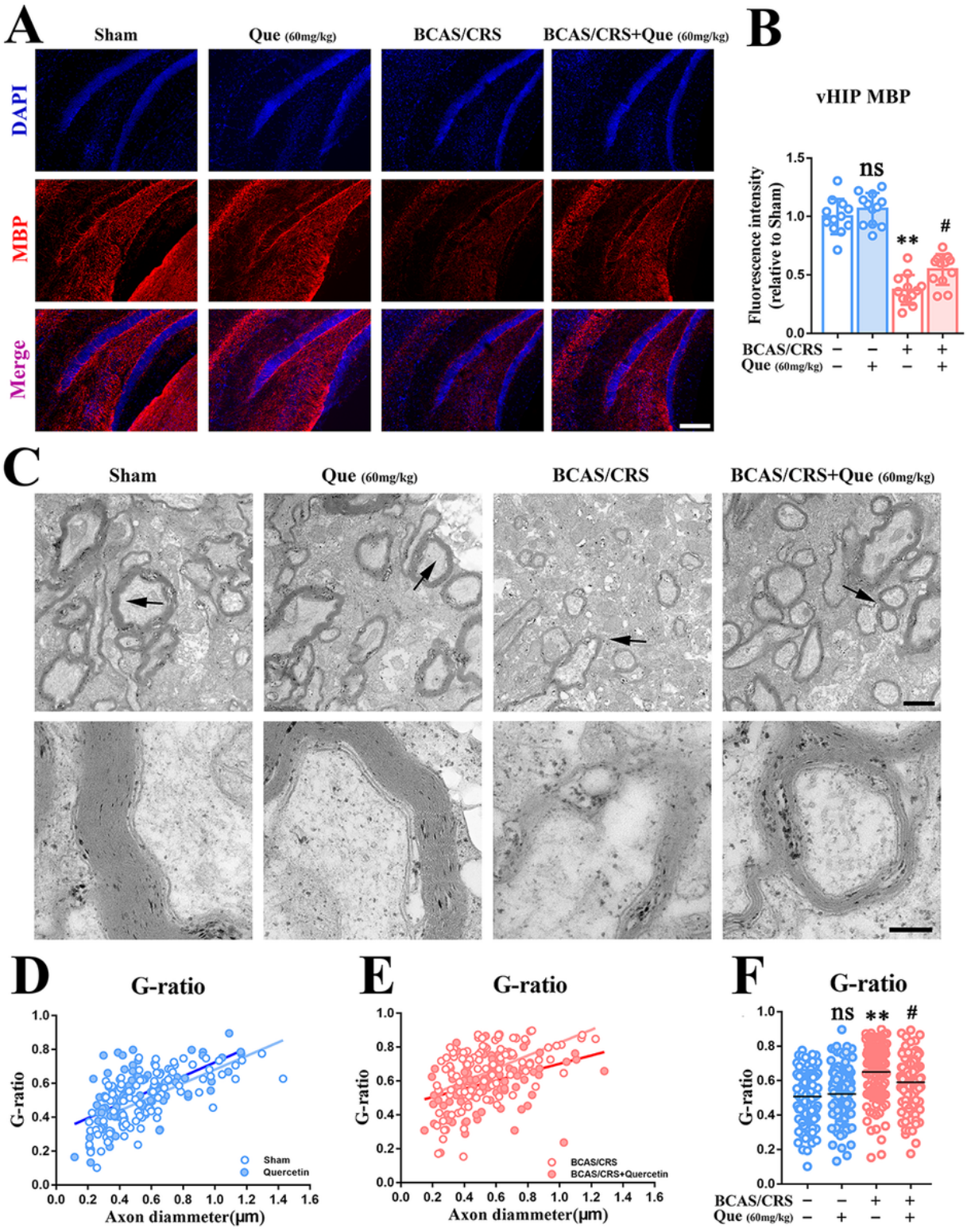

Figure 4

Quercetin restores hippocampal myelination in BCAS/CRS mice. (A) Typical immunostaining images of MBP at vHIP in each group. Cell nuclei were counterstained with DAPI. Scale bar: 200 μm. (B) Quantitative analysis illustrating the relative fluorescence intensity of MBP in different group. N=4 in each group, three brain slices per each sample were chosen for analysis. *p<0.05, **p<0.01 versus sham; #p<0.05, ##p<0.01 versus BCAS/CRS; ns, no significant difference. (C) Representative images of TEM

showing myelin in the vHIP in each group. Scale bar: 1 μm; and 200 nm in enlarged insert. (D) The efficiency index curves for axon caliber in groups Sham and Quercetin. (E) The efficiency index curves for axon caliber in groups BCAS/CRS and BCAS/CRS + Quercetin. (F) Quantitation of G-ratio representing the myelinated axons in each group. N=3 in each group, five horizons were chosen for analysis. **p<0.01 versus sham; #p<0.05 versus BCAS/CRS; ns, no significant difference.

Figure 5

Quercetin facilitates microglial M2 polarization in BCAS/CRS mice. (A) Bands depicting the protein expression of iNOS and Arg-1 in vHIP in different groups. (B) Semi-quantitative analysis of iNOS in each group. N=6 in each group, **p<0.01 versus sham; ##p<0.01 versus BCAS/CRS; ns, no significant difference. (C) Semi-quantitative analysis of Arg-1 in each group. N=6 in each group, ##p<0.01 versus BCAS/CRS; ns, no significant difference. (D) Representative immunostaining images co-labeled with Iba1 and iNOS. Cell nuclei were counterstained with DAPI. Scale bar: 100 μm; and 20 μm for enlarged inserts. (E) Histogram summarizing the percentage of iNOS+Iba1+/Iba1+ in different groups. N=4 in each group, three brain slices per each sample were chosen for analysis. **p<0.01 versus sham; ##p<0.01 versus BCAS/CRS; ns, no significant difference. (F) Typical immunostaining images co-labeled with Iba1 and Arg1. Cell nuclei were counterstained with DAPI. Scale bar: 50 μm; and 10 μm for enlarged inserts. (G) Histogram representing the percentage of Arg1+Iba1+/Iba1+ in different group. N=4 in each group, three brain slices per each sample were chosen for analysis. **p<0.01 versus sham; ##p<0.01 versus BCAS/CRS; ns, no significant difference.

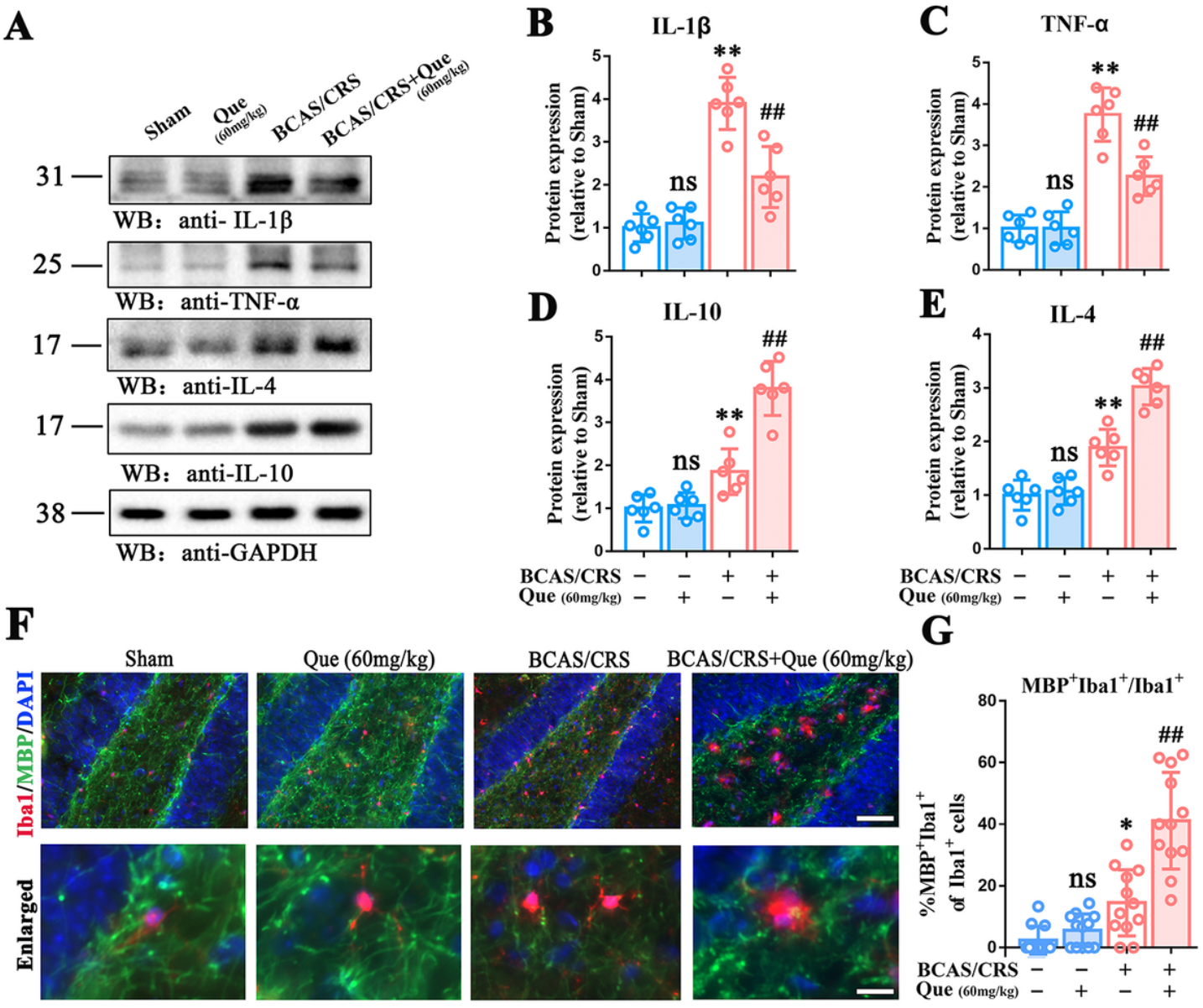

Figure 6

Quercetin improves the phagocytosis function of M2 microglia in the vHIP in BCAS/CRS mice. (A) Bands representing the expression of IL-1β, TNF-α, IL-10 and IL-4. (B-E) Semi-quantitative analysis illustrating the expression of IL-1β (B), TNF-α (C), IL-10 (D) and IL-4 (E). N=6 in each group, **p<0.01 versus sham; ##p<0.01 versus BCAS/CRS; ns, no significant difference. (F) Representative images of MBP and Iba1 in each group. Cell nuclei were counterstained with DAPI. Scale bar: 50 μm; and 10 μm for enlarged inserts. (G) Barchart demonstrating the percentage of MBP+Iba1+/Iba1+ in different groups. N=4 in each group, three brain slices per each sample were chosen for analysis. *p<0.05 versus sham; ##p<0.01 versus BCAS/CRS; ns, no significant difference.

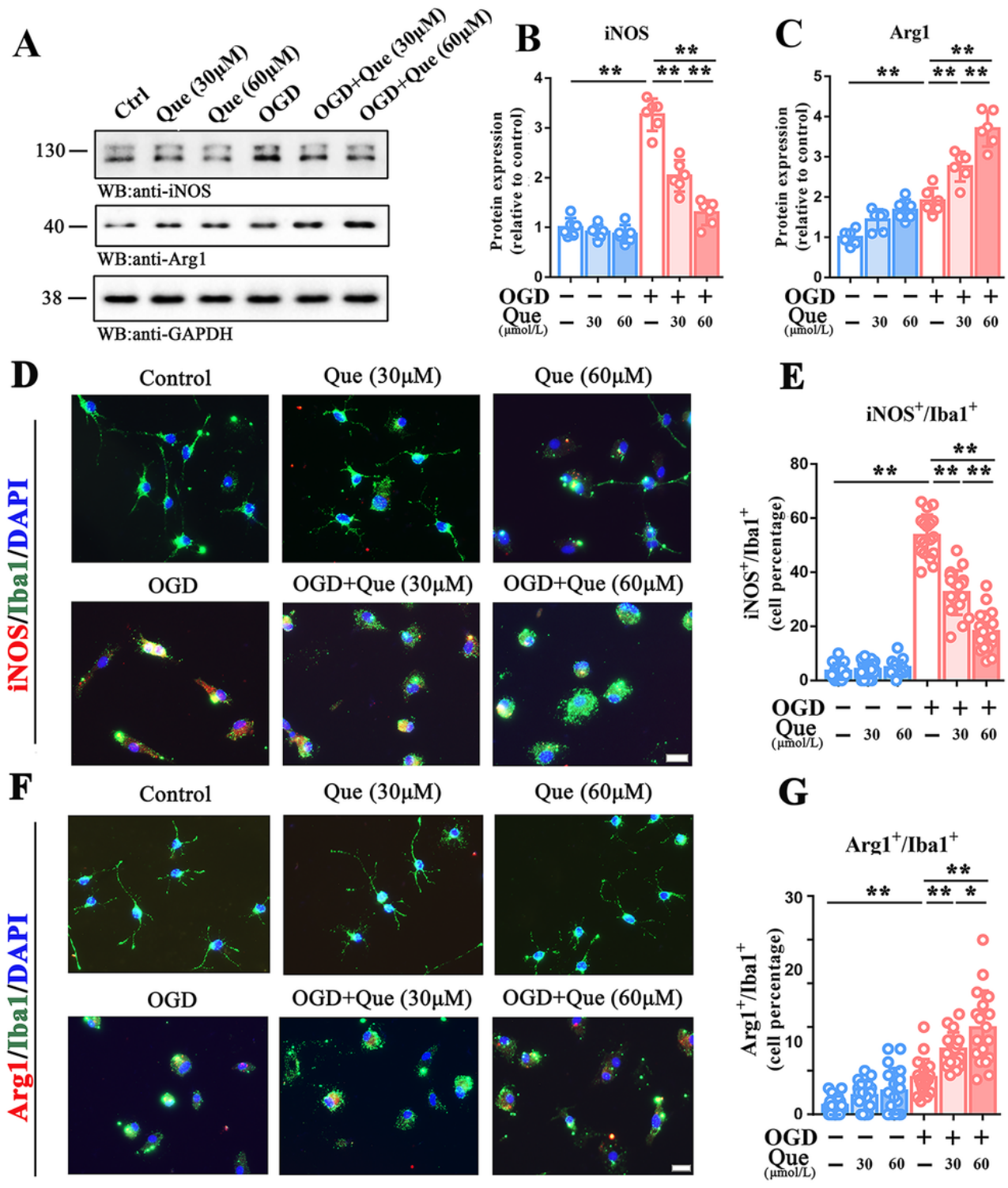

Figure 7

Quercetin promotes phenotypic transformation of primary microglia into M2 exposed to OGD in vitro. (A) Bands depicting the expression of iNOS and Arg-1 in primary microglia exposed to OGD in vitro. (B-C) Semi-quantitative analysis showing the expression of iNOS (B) and Arg-1 (C). N=6 in each group, **p<0.01. (D) Representative images of co-labeled with Iba1 and iNOS in each group. Cell nuclei were counterstained with DAPI. Scale bar: 25 μm. (E) Histogram summarizing the percentage of iNOS+/Iba1+

in different groups. N=6 in each group, three visions per each sample were chosen for analysis. **p<0.01. (F) Representative images of co-labeled with Iba1 and Arg1in each group. Cell nuclei were counterstained with DAPI. Scale bar: 25 μm. (G) Histogram summarizing the percentage of Arg1+/Iba1+ in different groups. N=6 in each group, three visions per each sample were chosen for analysis. *p<0.05, **p<0.01.

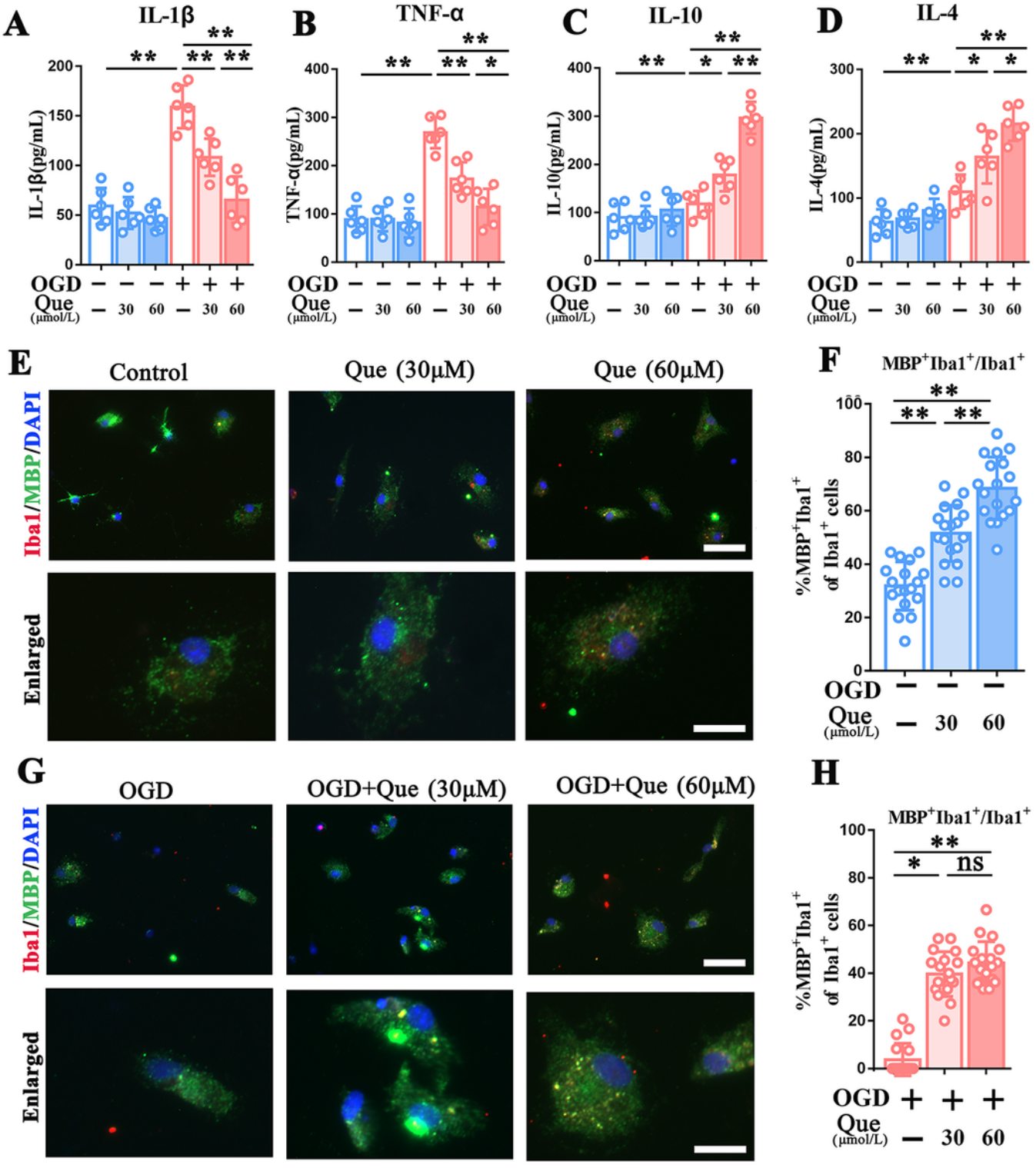

Figure 8

Quercetin suppresses the pro-inflammatory factors secretion and improves phagocytosis of primary microglia exposed to OGD in vitro. (A-D) The secretive concentration of IL-1β (A), TNF-α (B), IL-10 (C) and IL-4 (D) in supernatant using ELISA assays in each group. *p<0.05, **p<0.01. (E) Representative images of co-labeled with Iba1 and MBP in primary microglia without OGD exposure in each group. Cell nuclei were counterstained with DAPI. Scale bar: 50 μm; and 10 μm for enlarged inserts. (F) Bargraph summarizing the percentage of MBP+Iba1+/Iba1+ in different groups. N=6 in each group, three visions per each sample were chosen for analysis. **p<0.01. (G) Typical images of co-labeled with Iba1 and MBP in primary microglia with OGD exposure in each group. Cell nuclei were counterstained with DAPI. Scale bar: 50 μm; and 10 μm for enlarged inserts. (H) Histogram summarizing the percentage of MBP+Iba1+/Iba1+ in each group. N=6 in each group, three visions per each sample were chosen for analysis. *p<0.05, **p<0.01; ns, no significant difference.